CO_2 CORROSION OF THE WELDED JOINT OF AN X65 STEEL: ANALYSIS OF SURFACE FILM FORMED

A Thesis presented to the Department of

Materials Science and Engineering

African University of Science and Technology, Abuja

In Partial Fulfillment of the Requirements

For the Degree of

MASTER OF SCIENCE

BY

ADEBOLA, Titilope-Oluwa

DECEMBER, 2014

ABSTRACT

Carbon dioxide (CO_2) corrosion, also known as sweet corrosion of steels has increased in recent years due to the injection of CO_2 into oil wells in order to increase oil recovery and production. Despite the fact that carbon steel has a low corrosion resistance, it is widely used in the petroleum industry due to its economic advantage. It has been reported that when ferrous steels are exposed to a corrosive medium, they form a protective surface film which helps to decrease the rate of corrosion that would have occurred otherwise. It has been observed that many factors including; differences in chemical composition, temperature, flow rate, pressure and pH can affect the properties of the protective layer formed on the steel surface. A significant variation in microstructure contributes to localized corrosion due to non-homogenous surface film formation. Researchers have therefore emphasized the importance of understanding the specific nature of the film produced under certain conditions. This research aims at characterizing the surface film which forms across the welded joint of an X65 steel exposed to brine and CO_2 produced by sugar-fermenting yeast at 65^{o}C. SEM results showed that the film formed across the regions of the weld varied in the degree of protectiveness, which was responsible for the corrosion rates observed.

ACKNOWLEDGEMENT

This work would not have been possible without the support received from various people whom I am forever grateful to.

My sincere appreciation goes to my supervisor, Prof. W. O. Soboyejo for the support and mentorship. Despite his busy schedule, he always took his time to analyze my work and give constructive criticism and feedback. Thank you for your coaching and mentorship. I have learnt life-changing values simply from associating with you.

To Engr. Yusuf and his staff at the SCC steel company, I am grateful for the time you took in providing all the materials I needed to carry out this research. This work would not have been possible without your input.

To Prof. Zebaze Kana and the staff of Kwara State University, for the technical assistance rendered in this work. I am truly grateful.

To Mr. Shola Kolawole, Mr. Emmanuel Arthur and Mr. Edward Ampaw for taking time to critically review my work and offer both technical assistance and moral support through the challenges experienced during the cause of the research.

To Mr. Jerry in the Biochemistry Department at Nigerian Turkish Nile University, where I carried out my experiments. Thank you for granting me unrestricted access into your laboratory.

Finally to my fellow M.Sc colleagues at the Materials Science and Engineering Department, AUST, thank you for your support in one way or the other.

DEDICATION

This thesis is dedicated

to God, without whom this work would not have been,

to my family, for the unending love and support

and to Mr. Oluwashina Dada, my source of constant encouragement.

TABLE OF CONTENT

LIST OF FIGURES

LIST OF TABLES

CHAPTER 1: INTRODUCTION

1.1 BACKGROUND

Carbon dioxide (CO_2) corrosion has posed a serious problem to the oil and gas industry for over sixty years [13]. According to [52], approximately 70% of oilfield failures are related to CO_2 corrosion. This is due mainly to inadequate predictive capability and the poor resistance of carbon and low alloy steels to this type of corrosive attack. It causes both general and localized corrosion and is responsible for huge economic losses due to equipment failure [49]. Despite their low corrosion resistance, carbon and low alloy steels are widely used in the oil and gas industry due to their low cost and attractive combination of mechanical properties [50].

Localized CO_2 corrosion occurs commonly in carbon steels at welded joints. A welded joint consists of three layers; the parent metal (PM), the heat affected zone (HAZ) and the weld metal (WM) [47]. When galvanic corrosion occurs between the different regions of a weld, the resulting phenomena are characterized as preferential weld corrosion (PWC) [19]. PWC in carbon steels under sweet conditions has received considerable attention from researchers, as efforts are being made to develop ways of mitigating PWC.

The mechanism of CO_2 corrosion is highly complex, as it is largely influenced by the environmental conditions surrounding its occurrence [20]. Some of these conditions include: pH; temperature; flow-rate and microstructure of the metal [49]. During the process of CO_2 corrosion in steel, precipitates of iron carbonate, $FeCO_3$ accumulate over time, forming a protective film on the surface of the metal [13]. These films reduce the

corrosion rate significantly, thereby protecting the asset by extending the time to failure. The protective characteristics of the surface scale formed in CO_2 saturated brines depend on the nature of the base alloy and the environment [15]. Variations in the properties of the surface of steel (across a weld) are also responsible for the variations in the protective film that is formed across that region [18].

1.2 AIMS AND OBJECTIVES

Despite numerous CO_2 corrosion prediction models that have been developed, the level of accuracy in predicting the actual rate of CO_2 corrosion remains questionable. The interdependency of the various factors that contribute to CO_2 corrosion is responsible for the complexity.

Hence, though many models for predicting CO_2 corrosion take into account the influence of different environmental variables, the effects of steel microstructure and composition are only considered in a few of the models [15].

The objective of this research is to investigate the effects of variations in the microstructure of an X65 steel on the corrosive properties of $FeCO_3$ film. Variations in microstructure can be seen across the welded joint of a steel pipeline as a result of exposure to elevated temperatures during welding. This gives rise to three zones at the welded joint; parent metal, heat affected zone and weld metal. Film formation across each region of the weld will be analyzed in order to develop a basic understanding of film formation and PWC. The CO_2 gas that will be used in this study will be produced by sugar-fermenting yeast.

1.3 SCOPE OF WORK

This research will develop a fundamental understanding of the protective film that is formed across the welded joint of an X65 steel in the presence of CO_2. The protective film on the surface of the parent metal, heat affected zone and weld metal, will be characterized to determine the variations across the weld. Corrosion rates will also be measured for each region of the weld. Efforts will also be made to establish potential relationships between the measured corrosion rate and the film properties in the parent metal, heat affected zone and the weld metal.

1.4 OUTLINE OF THESIS

This chapter presents a brief overview on the background, research objective and the scope of the research. Chapter two presents an extensive literature review on CO_2 corrosion in the oil and gas industry. It also highlights the factors that contribute towards passive film formation in low carbon steels. Chapter three discusses in detail the experimental procedures that are used in promoting passive film formation in simulated CO_2-rich brine. Chapter four presents the results obtained from the experiments. Finally, salient conclusion arising from this work are presented in Chapter five along with recommendation for future work.

CHAPTER 2: LITERATURE REVIEW

2.1 INTRODUCTION

Welding causes significant variations to the microstructure of steels as a result of the cyclic heating and cooling which occurs during the process [20]. With the rise in the occurrence of corrosion at welds, it is imperative that researchers understand the factors that contribute to this phenomenon, in order to develop more effective methods of mitigation, as well as effective corrosion prediction models. CO_2 environments are extremely corrosive and have posed a challenge to the oil and gas industry for over sixty years [13]. The major concern with CO_2 corrosion is that it causes failure of equipment in the main down-hole tubing and transmission pipelines, thereby causing disruption in the production [15].

2.2 CORROSION

Corrosion is more frequently associated with metallic materials and involves material loss in the form of dissolution [47]. Metallic corrosion can be defined as a coupled electrochemical reaction consisting of an anodic metal oxidation and cathodic oxidant reduction [38]. Simply put, corrosion involves the transfer of electrons from one chemical species to another. It occurs in a variety of environments, ranging from aqueous to dry environments. Corrosion poses a serious economic problem to many industries, ranging from automobile to oil and gas industries. The process of corrosion can be explained using equation below [47];

$$M \rightarrow M^{n+} + ne^{-} \quad (2.2.1)$$

From the equation above, it can be seen that the metal (M), dissociates to form a positively charged ion with an oxidation number (n), corresponding to the number of valence electrons lost. After generation, these electrons must then be transferred to another chemical species in what is known as a 'reduction' reaction as shown below [47];

$$R^{n+} + ne^{-} \rightarrow R_n \quad (2.2.2)$$

The site where the metal dissolution occurs is known as the *anode* while that where reduction occurs is called the *cathode*. The predominant cathodic reaction that occurs in metals involve the reduction of hydrogen (H^{+}) ions and oxygen molecules [38]. The total electrochemical reaction is, therefore, the sum of the oxidation and reduction reaction as shown below;

$$M + R^{n+} \rightarrow M^{n+} + R_n \quad (2.2.3)$$

Corrosion can occur in various forms, depending on the nature of the material and environmental factors involved. Table 2.2.1 shows the different classifications of corrosion and examples of each. The five classifications of corrosion are: general corrosion; localized corrosion; metallurgically-influenced corrosion; mechanically assisted corrosion, and environmentally-induced cracking [40]. General corrosion is classified by uniform thinning of metal, while localized corrosion involves an increased corrosion rate at specific sites across the metal surface [39]. Metallurgically influenced corrosion involves all corrosion types which occur as a result of the microstructure of a metal.

Table 2.2.1 Classification of Corrosion Types [40]

]

General	**Localized**	**Metallurgically Influenced**	**Mechanically Assisted**	**Environmentally Induced Cracking**
Atmospheric	Crevice	Intergranullar	Erosion-corrosion	Stress- Corrosion Cracking (SCC)
Galvanic	Fillform	Dealloying	Fretting	Hydrogen Damage
Stray-current	Pitting		Corrosion fatigue	Liquid metal embrittlement
General biological corrosion	Localized biological corrosion		Cavitation and water drop impingement	Solid metal induced embrittlement
Molten-salt				
High-temperature				

2.3 CO_2 INJECTION FOR ENHANCED OIL RECOVERY

With the rapid depletion of oil reserves across the world, increasing the oil recovered from aging oil wells has become a major concern for oil companies [2]. Contrary to speculations made by the Worldwide Production Report in 1992, the rate of the replacement of depleted reserves with new discoveries has declined remarkably. After primary production, the most conventional method of secondary production being

employed is water flooding, which involves water being pumped into reserves, thereby pushing the oil to the surface (since water is denser than oil). Although water flooding has been able to recover a substantial amount of oil, the amount of oil that remains in the reservoir can be as high as 50% [1]. There is therefore a need to increase oil production from mature reserves. This has given rise to what is known as Enhanced Oil Recovery (EOR).

EOR simply comprises various techniques that are used to increase the amount of oil that can be extracted from an oil field after secondary production [5]. Some popular methods of EOR include: high pressure air injection (HPAI); steam injection; miscible gas injection, and chemical flooding [5]. CO_2 injection is preferred due to its high production efficacy and its contribution to greenhouse gas disposal [5]. The ratio of CO_2 injected to oil recovered usually lies between a range of 1:1 and 4:1 [1]. In addition, CO_2 gas can be readily available from power plants or industrial waste [4]. The gas is injected into existing wells or reservoirs to increase the pressure within these wells, causing the oil to rise to the surface [4]. It is believed that CO_2 injection has the potential to recover 15-20% of the left-over oil in mature reserves [4].

2.4 CO_2 /SWEET CORROSION

In oil wells, CO_2 gas dissolves in NaCl brine that is supplied with oil, to cause severe corrosion of steel pipelines that are used in the transportation of oil and natural gas [8]. The first encounter engineers had with CO_2 corrosion (or sweet corrosion as it is popularly referred to as), was in the 1940s at gas and gas-condensate fields of the USA [53]. Since then, scientists and engineers have been researching on ways to mitigate sweet corrosion, due to the high CO_2 content in oil and gas fluids, which can cause equipment failure [10]. Due to the fact that CO_2 gas is used in EOR, equipment used for this purpose is most affected by sweet corrosion. Equipment such as oil well pipes, transmission pipes and oil tubes have been reported to suffer from sweet corrosion [10, 11].

Sweet corrosion can occur on either the internal or exterior surface of a transportation pipeline. Internal corrosion can also occur as a result of dissolved CO_2 in NaCl brine during EOR, while exterior corrosion can occur as a result of the permeation of moisture, oxygen and CO_2 into the soil through a debonded coating [54]. Sweet corrosion, however, usually occurs in the absence of oxygen and is found to enhance the rate of general and localized corrosion [12].

The mechanism of sweet corrosion in oil and gas fields is extremely complex, as it is dependent on several interrelated factors. It is for this reason that different segments of the same unit (for example, a transmission pipeline), can experience different rates of corrosion [9]. It is generally accepted that CO_2 gas reacts with water to form carbonic acid, which will lower the pH of the solution, thereby increasing the corrosion rate [22].

However, due to its complex nature, a lot of unanswered questions have been raised regarding the exact mechanism of sweet corrosion [13]. The most popular mechanisms are those proposed by: De Waard and Milliams [55]; Schmitt and Rothmann [13,14] and George and Nesic [56]. The main similarity between these mechanisms is the fact that they all involve carbonic acid and bicarbonate ions formed during the dissolution of CO_2 in water [13].

The chemical reactions that occur in the system are presented below:

$$CO_{2_{(g)}} + H_2O \leftrightarrow CO_{2_{(dissolved)}} \quad (2.3.1)$$

$$CO_{2_{(dissolved)}} + H_2O \leftrightarrow H_2CO_3 \quad (2.3.2)$$

The CO_2 gas dissolves in water to form carbonic acid reaction in a two-step process. This reaction is followed by the carbonic acid dissociation:

$$H_2CO_3 \leftrightarrow H^+ + HCO_3 \quad (2.3.3)$$

$$HCO_3 \leftrightarrow H^+ + CO_3^{2-} \quad (2.3.4)$$

The electrochemical reactions that occur on the surface of the steel include: one anodic reaction and three cathodic reactions [13].

The anodic reaction is the dissolution of iron into ferric acid as shown below:

$$Fe \leftrightarrow Fe^{2+} + 2^{e-} \quad (2.3.5)$$

The cathodic reactions are:

$$2H^+ + 2e^- \leftrightarrow H_2 \quad (2.3.6)$$

$$2H_2CO_3 + 2e^- \leftrightarrow H_2 + 2HCO_3^- \quad (2.3.7)$$

$$2HCO_3^- + 2e^- \leftrightarrow H_2 + 2CO_3^{2-} \quad (2.3.8)$$

The predominant cathodic reaction is dependent on the pH of the corrosive environment, as illustrated in Table 2.4.1. It has been experimentally proven that carbonic acid solutions are more corrosive than solutions of stronger acids at the same pH value [9].

Table 2.4.1 Cathodic Reaction at Various pHs [51]

pH Range	**Predominant Cathodic Reaction**
< 4	Hydrogen reduction
4 - 6	Carbonic acid reduction
> 6	Bicarbonate ion reduction

2.5 PROTECTIVE FILM FORMATION (PASSIVATION)

Film formation occurs following the electrochemical reactions that occur during CO_2 corrosion. When the concentration of ferric ions (Fe^{2+}) and bicarbonate ions (CO_3^{2-}) in the solution exceed the solubility limit, precipitation of iron carbonate occurs as shown below [15]:

$$Fe^{2+} + CO_3^{2-} \rightarrow FeCO_3 \quad (2.5.1)$$

$$Fe^{2+} + 2HCO_3^- \rightarrow Fe(HCO_3)_2 \quad (2.5.2)$$

$$Fe(HCO_3)_2 \rightarrow FeCO_3 + CO_2 + H_2O \quad (2.5.3)$$

The $FeCO_3$ precipitates build up over time and can act in a protective or non-protective manner, depending on the exact conditions in which they are formed [13]. The type of film formed is, therefore, strongly dependent on the nature of the surrounding environment. These conditions include: temperature, pH, flow-rate, pressure, microstructure and composition [36]. The driving force for precipitation of $FeCO_3$ is super-saturation and precipitation occurs in two steps; nucleation and particle growth [48]. Due to the fact that precipitation proceeds at a very slow rate, a high degree of super-saturation will ensure $FeCO_3$ will deposit on the metal surface [48]. The solubility limit (Ksp_{FeCO3}) and super-saturation (SS) are related via the equation [25]:

$$SS = \frac{[Fe^{2+}][CO_3^{2-}]}{[Ksp_{FeCO3}]} \quad (2.5.4)$$

where SS = Super-saturation, Ksp_{FeCO3} = Solubility limit, $[Fe^{2+}]$ and $[Co_3^{2-}]$ = ferrous and carbonate ion concentration respectively [25].

Scale precipitation will occur when the value of SS exceeds unity [25]. According to Johnson and Thompson, the super-saturation and temperature are the two most important factors which affect the rate of precipitation of iron carbonate [37].

The protective film creates a diffusion barrier for the corrosive specie and prevents electrochemical reactions from occurring underneath it. It could form in a homogenous or non-homogenous manner, which will determine the degree of coverage of the surface of the metal. A non-homogenous film will induce localized corrosion on the metal surface, whereas a homogenous film will prevent further dissolution of the metal [13]. Researchers have, therefore, emphasized the importance of understanding the effects of these environmental conditions on the nature of the protective film formed [13].

When the iron carbonate precipitates form a protective film on the surface of a metal, the corrosion rate is significantly reduced [48]. Hausler and Stegmann [11] emphasized the importance of understanding the microstructure and characteristics of the protective film formed as a result of sweet corrosion under certain conditions. According to Van Hunnick et al., the rate of precipitation of the $FeCO_3$ film can be expressed as:

$$R_{FeCO_3} = \frac{A}{V}.f(T).K_{sp}.f(SS) \quad (2.5.5)$$

Where A is the surface area of exposed sample, V is the volume of solution, K_{sp} is the $FeCO_3$ solubility limit, SS is the super-saturation.

2.6 FACTORS THAT AFFECT FILM FORMATION

There are several factors that determine the properties of protective film that form across the surfaces of metals. These factors are responsible for the homogenous or non-homogenous nature of the films [13]. The effects that these conditions have on film formation are highlighted and discussed in this chapter.

2.6.1 TEMPERATURE

Temperature plays a crucial role in the precipitation and stability of iron carbonate film. Iron carbonate solubility decreases with increasing temperature [13] and this allows for precipitates to form more easily at higher temperatures. As a result, protective films form more readily at temperatures above 60^{o}C [15]. This temperature is referred to as the *maximum scaling temperature*, which is dependent on several factors [57].

At temperatures below 40^{o}C, the precipitation rate of $FeCO_3$ is extremely slow and can take weeks to form [49]. The morphology of the film formed at different temperatures varies significantly. At temperatures above 90^{o}C, the film has a well-defined cubic structure, while at lower temperature the surface consists of flat grains [49]. The surface film morphology is not solely dependent on the temperature however, as the pH and CO_2 partial pressure are also important.

2.6.2 pH Effects

An increase in pH leads to a decrease in the uniform corrosion rate by influencing the electrochemical mechanisms and iron carbonate formation [15,48]. This is largely due to the decrease in the solubility of $FeCO_3$ and the formation of carbonate and bicarbonate salts. The cathodic reduction of H^+ slows down, thereby decreasing the anodic dissolution rate of iron at high pH [49].

Despite the fact that the pH gives an indication of the corrosivity of the electrolyte, it cannot be used to directly predict the occurrence of protective corrosion product films [48]. In certain circumstances, the film formed can lead to an increase in corrosion rate irrespective of favorable pH [50].

2.6.3 Microstructure

The microstructure is important because it determines how well the protective film will adhere to the surface of the metal [15]. It depends not only on the chemical composition, but also on the thermo-mechanical treatments employed during processing [15]. Researchers have shown that carbon steels with the same chemical composition, but different microstructures can have varying corrosion rates [58]. The effect of microstructure is strongly attributed to the roles of different phases in acting as anodic or cathodic sites [49].

The microstructure of low alloy steels is usually composed of proeutectoid ferrite and pearlite [16]. In steels with a ferritic-pearlitic structure, the $FeCO_3$ film is better anchored on the metal surface [59]. This is due to the fact that ferrite is more anodic than

cementite, Fe_3C. The ferrite will, therefore, corrode preferentially with respect to the cementite [16]. Ferrite is located within the pearlitic matrix and, therefore, deposits of carbonate adhere to the cementite, which is located at the surface of the metal when the ferrite corrodes [13]. This will only occur when the Fe^{2+} and CO_3^{2-} ions exceed their solubility limit.

When carbonate adheres to the surface of the cementite, it forms a porous film which still permits further carbonate ions to penetrate through, thereby reacting with the metal [13]. This will allow further $FeCO_3$ precipitation, giving rise to a dendritic structure, which is less porous than the initial film formed [59]. This penetration and further corrosion will continue, until the $FeCO_3$ scale becomes thick and dense enough to provide maximum protection to the metal surface. It should be noted, however, that the accumulation of carbides in the corrosion product has been seen as the cause of increasing corrosion rate over time of exposure for ferritic-perlitic steels [15].

In steels with martensitic-bainitic microstructures, the Fe_3C distribution is less continuous and less ordered than that found in ferritic-pearlitic steels. The microstructure is, therefore, less efficient in anchoring $FeCO_3$ deposits on the surface of the metal [50]. According to Arne Dugstad, plain normalized steel with a ferritic-pearlitic microstructure has a better CO_2 corrosion resistance than quenched and tempered alloy steel with a martensitic microstructure [58]. The microstructure of the metal surface will determine the anchor of the protective film on the metal surface [13]. It should be noted that the microstructure of a metal can be altered by exposure to high temperature and/stress.

2.6.4 CHEMICAL COMPOSITION

Beyond microstructure, passivation also depends on the chemical composition of the steel. The two terms are often mistaken to be interdependent, however researchers emphasize their independence [15]. Steels with the same chemical composition can have different microstructures and vice-versa. Researchers have shown that to obtain optimum corrosion resistance, addition of chromium (Cr) is of great importance [49]. An increase in *Cr* content leads to an increase in corrosion resistance of low alloy steels. This is because *Cr* forms a passive oxide layer on metal surfaces which reduces the corrosion rate. The amount of *Cr* alloyed into a metal is essential, due to the fact that a high *Cr*-content could lead to carbide formation at the grain boundary, thereby reducing the amount of *Cr* available for oxide film formation, and reducing the carbon content in the steel [49]. High *Cr* content also increases the susceptibility to pitting corrosion and stress corrosion cracking (SCC) in the presence of chlorides and small amounts of oxygen.

In order to avoid chromium carbide formation, additional alloying elements are added to metals which form stable carbides. These microalloying elements include; V, Ti, Mo, Nb, Cu and Si. Addition of elements like Ni, Mo and Cu improves a metals SCC resistance [49].

2.6.5 CO_2 PARTIAL PRESSURE

Generally, an increase in CO_2 partial pressure will lead to an increase in the rate of reduction of carbonic acid, thereby increasing the uniform corrosion rate [15]. This effect is dependent on other environmental conditions, such as pH and will occur during the formation of non-protective surface films [49].

De Waard-Millams proposed an equation relating the partial pressure to the corrosion rate as shown below [36];

$$logV_{corr} = 5.8 - \frac{1710}{273+T} + 0.67 \log (pCO_2) \qquad (2.5.5.1)$$

where V_{corr} is the corrosion rate, T is the temperature, and pCO_2 is the CO_2 partial pressure. The limitation of the above equation is that it does account for the effect of non-ideality of the gas phase and scale formation.

In environments which favor the formation of protective films however, an increase in CO_2 partial pressure will lead to a decrease in the corrosion rate [49]. This is due to the low availability of cathodic sites for the reduction of carbonic acid. It can be seen that the anodic reaction is unaffected by a change in partial pressure, whereas the cathodic reaction is affected. This relationship between partial pressure and corrosion rate which greatly varies, depending on the corrosive environment makes it difficult to establish a correlation between the two parameters.

2.6.6 FLOW

An increase in the flow velocity will lead to an increase in the corrosion rate. This is due to the fact that an increase in flow velocity will slow down the formation of the protective $FeCO_3$ film [15]. In a pipe containing fast moving fluid, the corrosion products are eroded, due to increased shear stress exerted against the pipe walls. Depending on the amount of particles in the fluid, existing films can also be delaminated through erosion-corrosion [50]. This will prevent re-formation of the film and increase metal dissolution [49]. High flow velocities can increase the removal of Fe^{2+} ions from the bottom of surface pores. This affects the super-saturation in those sites leading to slower precipitation rates, thereby affecting film formation.

2.6.7 OXYGEN CONTENT

CO_2 corrosion in carbon steels occurs in anaerobic environments i.e. the absence of oxygen [11]. Likewise, the $FeCO_3$ film which forms on the metal surface is highly unstable in the presence of oxygen [15]. This is due to the fact that oxygen promotes the oxidation of ferrous ions (Fe^{2+}) into ferric ions (Fe^{3+})[30]. The presence of oxygen promotes localized attacks [49].

2.6.8 ION CONCENTRATION

The ion concentration affects the super-saturation level and the corrosion rate. The amount of Fe^{2+} present in a CO_2-rich environment will determine the corrosion rate. At low Fe^{2+} concentrations, the corrosion rate will be high whereas a high concentration will lead to super-saturation and subsequently precipitation of $FeCO_3$ [49]. The presence of other cations also enhance scale formation.

2.7 WELDING

Welding is a joining process whereby two or more metal parts in contact with each other, are exposed to a suitable amount of heat and/or pressure in order to form a permanent joint between them [41].These parts could either have similar composition and structure, or be completely dissimilar. The microstructure and surface composition of welds and adjacent base metals can be affected by the cyclic heating and cooling associated with welding [20].

A weld consists of three regions namely; the parent/base metal (PM), heat-affected zone (HAZ) and weld metal (WM). These regions can be further sub-classified into five microstructurally distinct regions namely; the fusion zone, the unmixed region, the partially unmixed region, the HAZ and the unaffected parent metal as shown in Figure 2.6.1. It should be noted that the five zones are not always present in any given weld, as it is dependent on the method of welding employed. A weld which contains no filler metal (a metal added to the joint when welding), will not contain an unmixed zone. The parent metal is the metal which is to be welded and is present in the largest proportion. Its composition and microstructure is independent of the welding process. The fusion zone

occurs as a result of total melting of the parent metal with or without a filler metal. The composition and microstructure of the fusion zone is mostly different from that of the parent metal. This could induce a micro-galvanic couple between the two regions depending on the magnitude of the variation in their electrode potentials. The HAZ is the region of the weld that has been exposed to temperatures high enough to induce a microstructural change but too low to cause melting [20]. Therefore, the microstructure of the HAZ, WM and PM will be dissimilar, following welding.

There are various types of welding techniques that are used to create welds which have mechanical properties similar or superior to that of the parent metal [23]. The various welding techniques have been classified into two groups by the American Welding Society (ASM) namely; fusion welding and solid-state welding [41]. Fusion welding involves the application of heat in order to melt the parent metal, whereas solid-state welding involves the use of low-temperature (below the melting temperature of the metal) and/or pressure. Examples of popular welding techniques include: submerged-arc welding (SAW); gas metal arc welding (GMAW); oxy-fuel gas welding (OFW) and ultrasonic welding (USW).

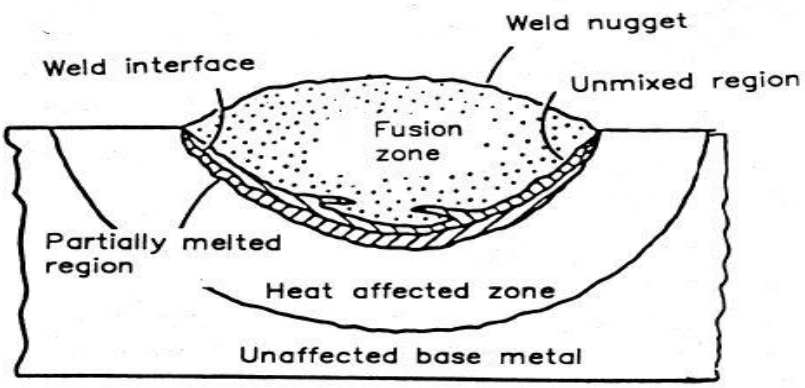

Fig. 2.6.1 Microstructural regions of weld [20]

2.8 PREFERENTIAL WELD CORROSION

Preferential weld corrosion (PWC) of carbon and low alloy steels used for pipelines, in CO_2 containing media, has been observed in recent years [18]. Simply put, PWC is a form of severe localized corrosion which occurs at welds [19]. It is the selective dissolution of metals associated with welds [21]. A galvanic couple can exist between the different regions of a weld, due to their different potentials. This is as a result of a more anodic WM and HAZ than the PM [19]. As a result of the small surface area of the WM and HAZ, as opposed to that of the PM, the rate of galvanic corrosion is very high. Severe PWC in carbon steel is illustrated in Figure 2.6.2 [22].

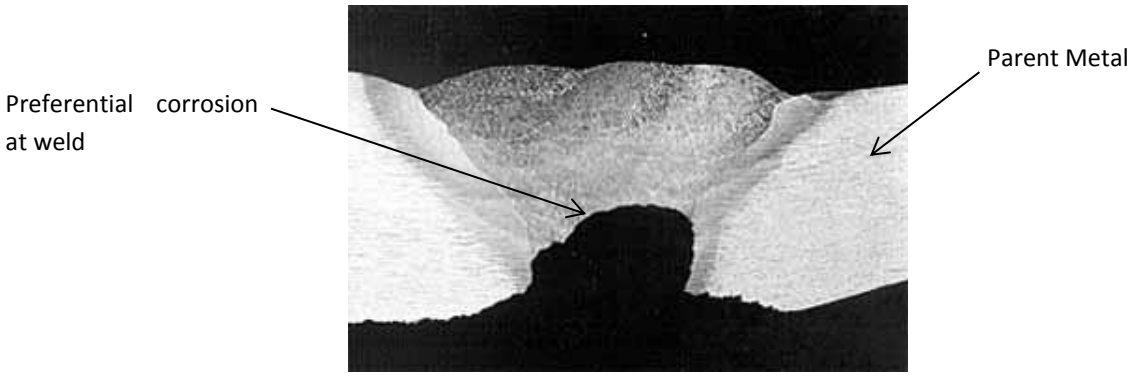

Fig. 2.6.2 PWC in carbon steel [22]

PWC in CO_2 environments is influenced by a complex interaction of several conditions which include: temperature, welding procedure and parent steel composition [18]. No general agreement exists on the role of alloying elements and microstructure in preferential weld corrosion [18].

Welding causes variations in the microstructure and/or composition of a metal. As a result of the variations in microstructure across a weld, corrosion product layers with varying degrees of thickness and protective properties are formed across the weld [17]. This variation in the protective film can contribute to localized corrosion at welds [13].

2.9 METHODS OF MITIGATING PWC

The most cost effective and versatile method of PWC mitigation is the use of inhibitors [26]. This could be applied through either continuous or batch treatment. As the name implies, continuous treatment involves constant injection of an inhibitor into oil and gas fluids. The major setback with inhibitors is their selectivity to various corrosion

environments. In other words, an inhibitor may be applicable in one oil and gas field, but inapplicable in another with different conditions.

Another method of PWC mitigation is the use of cathodic filler materials in weld consumables [49]. This involves the addition of noble metals; such as Ni and Cr, to the weld consumable [18]. Since galvanic coupling can exist between the weld metal and the parent metal, it is essential to ensure that the region with a lower surface area be more cathodic, so as to reduce the corrosion rate [19]. The addition of noble metals to the weld metal (which has a smaller surface area compared to the parent metal), will make it more cathodic with respect to the PM. It should be noted however, that 'over-alloying', could have a detrimental effect on the preferential corrosion rate, as it can induce attach of the HAZ [18].

2.91 CORROSION PREDICTION MODELS

There are two types of models that exist for predicting sweet corrosion: empirical and mechanistic models [10]. The empirical model is typically derived from correlation of experimental data only. The mechanism of corrosion has little or no impact on the model derivation [10]. The mechanistic model on the other hand, is derived from first principles and takes into account, the mechanism of corrosion [10].

Despite the numerous prediction models that exist however, the existing models are unreliable in predicting the actual CO_2 corrosion resistance of low alloy steels [15]. Recently, a mechanistic model was presented by Nordsveen et al. for CO_2 corrosion with protective iron carbonate films [60]. From the model, it was pointed out that the effects

due to the presence of conducting iron carbide surface films need to be introduced in order to obtain more accurate predictions.

CHAPTER 3: EXPERIMENTAL METHODS

3.1 INTRODUCTION

In order to prepare and analyze the $FeCO_3$ protective film that forms across a welded joint, the sample must be adequately prepared and exposed to a simulated sweet environment. Experiments were, therefore, conducted to ensure film formation and characterization.

3.2 EXPERIMENTAL PROCEDURES

This section presents the steps taken to: simulate a 'sweet' environment; promote film formation in various regions of the weld, and analyze film properties.

3.2.1 SAMPLE PREPARATION

Samples of the tube wall and welded joint of an X65 steel pipeline were cut from a spiral welded joint of the pipe. The pipeline was welded using the submerged arc welding (SAW) technique. In the SAW process, both the weld electrode and base metal are melted beneath a layer of flux [17]. The electrode used was Ba-s2Mo and the flux was Lincolnweld SPX80, The role of the flux is to protect the weld metal from contaminants and localize the heat at the joint. The welding was done on the internal and external region of the pipe, in order to complete the joint. This was responsible for the 'double V-

shape' of the weld joint as shown in Figure 2.9.1. The chemical analysis of the parent metal and weld metal are shown in Table 2.9.1. The chemical analysis technique used was the spark and arc atomic emission spectroscopy.

The samples were cut to dimensions of 20 x 40 x 7.5 mm^3, so that the weld metal was located at the center and later grinded and polished down to 600 grit size. After etching with nital solution, the three weld regions (PM, BM and HAZ), became visible and were later cut into a cuboidal geometry with exposed surface areas of 0.56, 0.70 and 0.55 mm^2 respectively. The individual weld regions were separated and chemical analysis carried out to ascertain the chemical composition of the parent metal and weld metal.

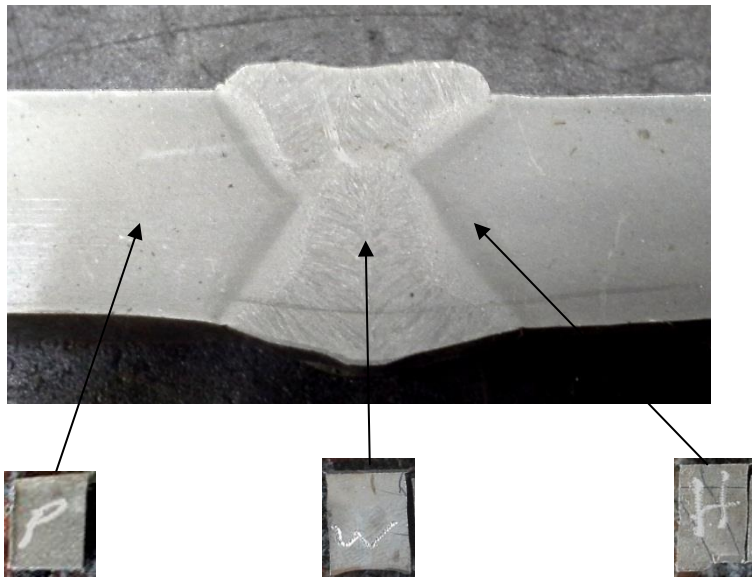

Fig. 2.9.1 Welded Joint of X65 Steel

Table 2.9.1 Chemical analysis of parent metal

C%	Si%	Mn%	P%	S%	Cr%	Mo%	Ni%	Al%	Cu%	Fe%
0.074	0.216	1.554	0.012	0.004	0.014	<0.002	<0.002	0.048	**0.011**	97.987

Table 2.9.2 chemical analysis of weld metal

C%	Si%	Mn%	P%	S%	Cr%	Mo%	Ni%	Al%	Cu%	Fe%
0.063	0.258	1.577	0.012	0.005	0.017	0.169	<0.002	0.023	0.024	97.791

3.2.2 PREPARATION OF CO_2 GAS

CO_2 gas was prepared by dissolving 125 g of sugar and 6 g of baker's yeast in two 1.5 L plastic bottles respectively. The plastic bottles each contained 850 ml of tap water. A hole was inserted into each of the bottle caps, through which a Ø 6 mm silicon tube was passed through. The tubes were connected to a 750 ml plastic bottle which had been rinsed with acetone to remove all traces of liquid. Three equally spaced holes were inserted into the cap of the 750 ml bottle, through which a Ø 6 mm silicon tube was passed through. These tubes would then act as a channel for the gas to the corrosion setup. The 750 ml bottle acted as a tank for the gas collection.

Yeast reproduces anaerobically in the presence of yeast and sugar to produce ethanol and carbon dioxide as shown in the equation below;

$$C_6H_{12}O_6 \rightarrow 2C_5H_5OH + CO_2 \quad (3.2.3.1)$$

In order to confirm that the produced gas was CO_2, the gas was purged into a solution containing 30 ml of distilled water for 24 hours. This was done to produce carbonic acid (equation 2.3.2). The solution was then titrated into a beaker containing 10ml of 2M NaOH solution, which had been stained with phenolphthalein indicator. Titration was continued until the solution became colorless, indicating the NaOH solution had been neutralized by the produced carbonic acid.

3.2.3 PREPARATION OF $FeCO_3$ FILM

Three simultaneous setups labeled Setups 1, 2 and 3 respectively, were constructed for this experiment. Each setup consisted of 50 ml of the base solution (pH 9.5) placed in an Erlenmeyer flask, respectively, which was then purged with CO_2 for 24 hours. The chemical composition of the base solution is shown in Table [3.2.3.1]. Each setup contained one parent metal, weld metal and heat affected zone which were placed into the solution after CO_2 purging. Prior to immersion, test samples were rinsed with acetone, followed by ethanol. The pH value was measured using a Vernier LabQuest pH meter. This was done at regular time intervals for the duration of the experiment to observe pH fluctuations. A continuous flow of CO_2 was maintained throughout the duration of the experiment. Corrosion in setups 1, 2 and 3 was carried out for 168 h. The samples were exposed to a temperature of 65^{o}C for the duration of the experiment

Fig. 3.2.3.1 Experimental Setup

Table 3.2.3.1: Chemical Composition of Base Solution [25]

Reagent	Concentration (g/L)
$CaCl_2$	0.0186
NaCl	0.5900
$MgCl_2.6H_2O$	0.0776
$NaHCO_3$	0.1245
Na_2SO_4	0.0078

3.2.4 WEIGHT LOSS

Weight loss experiments were used to determine the corrosion rates. The samples were weighed before being immersed into the corrosive media. Before being weighed, test samples were rinsed with distilled water and ethanol. Samples in setups 1, 2 and 3 were weighed, respectively, at 24 h intervals for 7 days. From weight loss measurements, the corrosion rates were obtained from:

$$R_{corr} = \frac{8.76*10^4*\Delta W}{\rho A t} \quad (3.2.5.1)$$

where; R_{corr} is the corrosion rate (mm/year), ΔW is the Change in mass (g), ρ is the density (g/cm^3) (7.85 g/cm^3), A is the Area of exposed surface in cm^2 and t is the time in hours [13].

3.2.5 SCANNING ELECTRON MICROSCOPY WITH ENERGY DISPERSED X-RAY SYSTEM

SEM imaging was done on the sample to view the surface morphology of the $FeCO_3$ film and the carbide structure of the steel surface. After corrosion, test samples were rinsed with distilled water and view under the SEM. Secondary imaging was done using Aspex 3020 PSEM2 SEM.

3.2.6 MICROSTRUCTURAL ANALYSIS

Microstructural analysis was carried out on each region of the weld prior to corrosion, to know the microstructure of the samples. Knowledge of the microstructure will give an idea of the nature of film anchorage to expect on each test sample. This will also determine the degree of coverage of the film on the surface of the metal. Test samples were once again grinded, polished and etched before being viewed under an optical microscope at a magnification of 400 X. The average pearlite grain sizes were measured using Gwyddion 2.39 software.

CHAPTER 4: RESULTS AND DISCUSSION

4.1 INTRODUCTION

Results obtained from the experimental work carried out are reported in this chapter. Implications of the obtained results are also discussed.

4.2 MICROSTRUCTURAL ANALYSIS

Microstructures of steel samples are indicated in Figure 4.2.1. It was observed that the PM, WM and HAZ each possessed a ferrite pearlite microstructure, which is the predominant phase in low carbon steels. Variations existed in the grain sizes and distribution. The HAZ possessed the largest average pearlite grain diameter of 2.23 μm. The WM had an average pearlite diameter of 1.02 μm, while the PM had an average pearlite diameter of 0.88 μm.

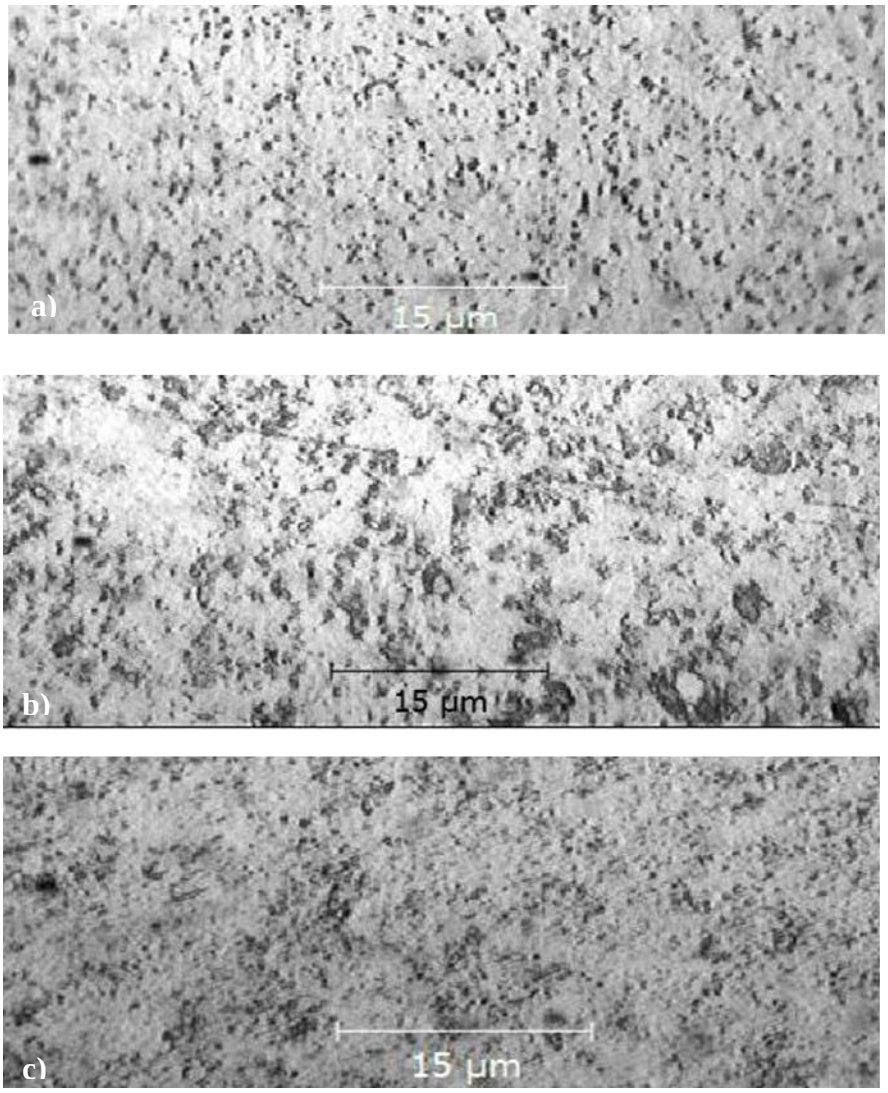

Fig. 4.2.1 Optical Micrograph of microstructures of a) WM, b) HAZ and c) PM after CO_2 corrosion at 400 X prior to CO_2 corrosion

4.3 WEIGHT LOSS

The corrosion rate patterns for the exposed samples are shown in Figure 4.3.1. The results indicate that the HAZ had the highest initial corrosion rate, as opposed to the PM and WM. This is followed by a subsequent decrease in the corrosion rate of the HAZ that

continues for the duration of the experiment. The WM was observed to have the lowest initial corrosion rate as opposed to the PM and HAZ. Corrosion rate in the WM decreases gradually and steadily for the duration of the experiment. The corrosion rate of the PM decreased at a lower rate for the duration of the experiment. After 168 h of exposure, the PM had the highest corrosion rate, while no corrosion was observed in the WM. Details of the mass loss and corrosion rate of each test sample for the duration of the experiment are summarized in Table 4.3.1

The pH variations with respect to time, for the exposed samples are shown in Figure 4.3.2. Prior to CO_2 purging into the base solution for 24 h, the pH of all solutions was 9.5. Following gas purging, the pH was seen to decrease in all solutions to a value of 6.5 ± 0.2, as shown in Table 4.3.2 indicating that the production of carbonic acid had occurred. pH measurements of the test samples for the duration of the experiment indicated that the predominant cathodic reaction was bicarbonate ion reduction.

Table 4.3.1 Corrosion Rate of Test Samples

Time (h)	Parameters	P	W	HAZ
24	**ΔM (g)**	0.002	0.002	0.002
	R_{corr} (mm/y)	1.660	1.329	1.691
48	**ΔM (g)**	0.003	0.003	0.002
	R_{corr} (mm/y)	1.245	0.996	0.845
72	**ΔM (g)**	0.004	0.003	0.002
	R_{corr} (mm/y)	1.107	0.664	0.564
96	**ΔM (g)**	0.004	0.003	0.002
	R_{corr} (mm/y)	0.830	0.498	0.423
120	**ΔM (g)**	0.003	0.003	0.002
	R_{corr} (mm/y)	0.498	0.339	0.338
168	**ΔM (g)**	0.004	0	0.002
	R_{corr} (mm/y)	0.474	0	0.242

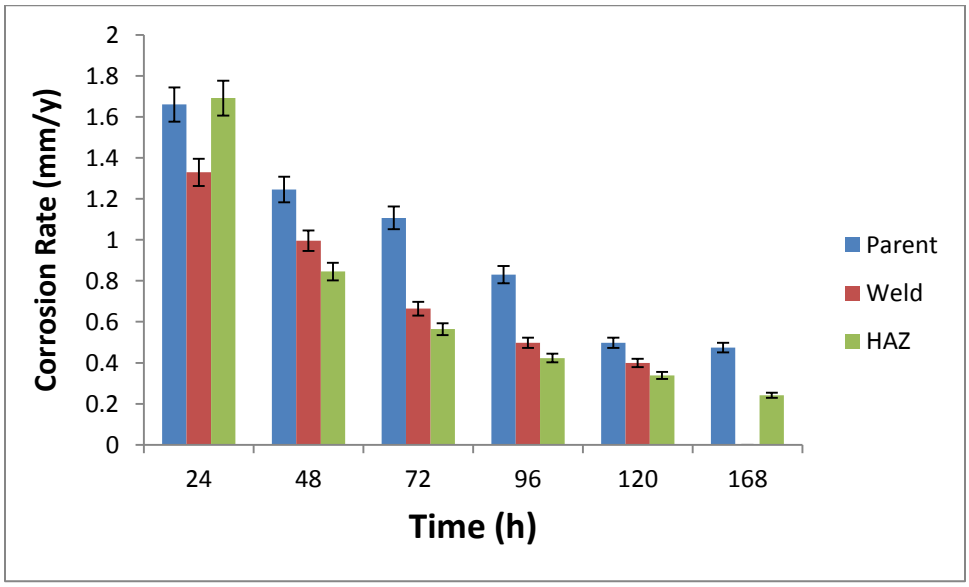

Fig. 4.3.1 Graph of Corrosion Rate vs Time for test samples

Table 4.3.2 pH of Test Samples

Time (h)	pH		
	P	**W**	**HAZ**
0	6.571	6.398	6.513
24	6.713	6.500	6.750
48	6.625	6.620	6.650
72	6.652	6.840	6.832
96	6.880	6.552	6.861
120	6.570	6.836	6.729
168	6.989	7.327	7.431

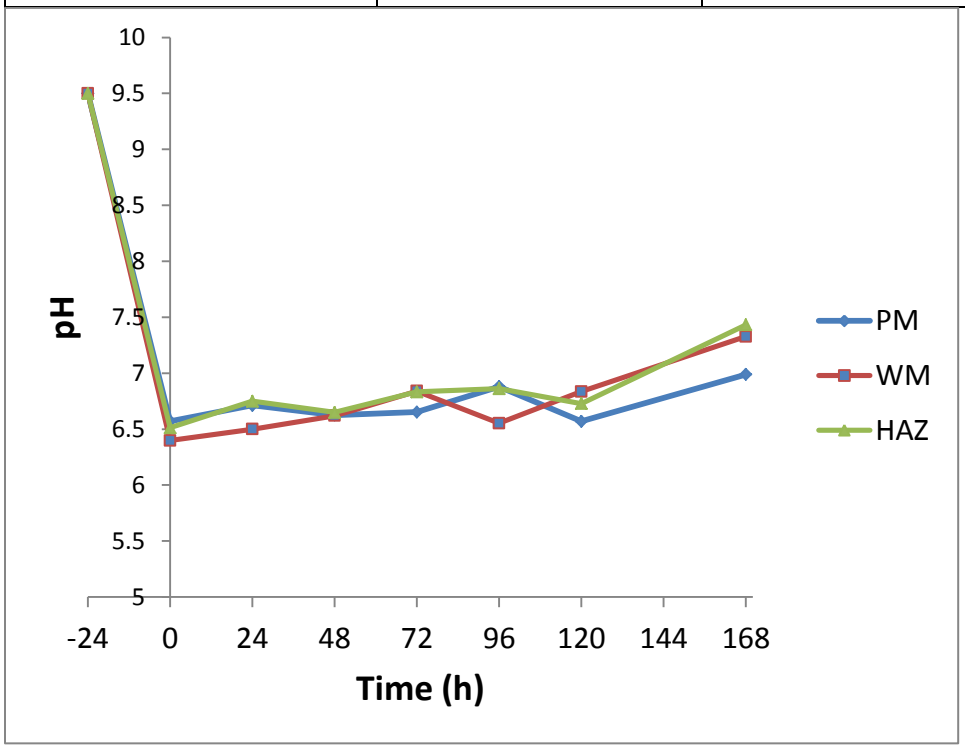

FIG. 4.3.2 Graph Showing the pH of Base Solutions

4.4 SEM IMAGING

Figure 4.4.1 shows the surface morphology of the parent, weld metal and heat affected zone after corrosion. $FeCO_3$ precipitates having a rhombohedric crystal structure, can be seen on the WM and HAZ surface forming a layer on the metal surface with varying degree of compactness.

It was observed that $FeCO_3$ deposition was more uniform across the surface of the weld metal, as opposed to that of the HAZ. This was evident from the compact network of precipitates forming a protective film on the weld surface. $FeCO_3$ precipitates in the WM and HAZ were measured to be about 1.54 µm in diameter. $FeCO_3$ precipitation occurred directly and integrated within the carbide phase of the WM and HAZ due to the cathodic nature of Fe_3C. The surface film on the HAZ was observed to have inclusions indicating sites where localized corrosion could occur. $FeCO_3$ scales were not observed on the surface of the parent metal, rather a porous network of Fe_3C was seen.

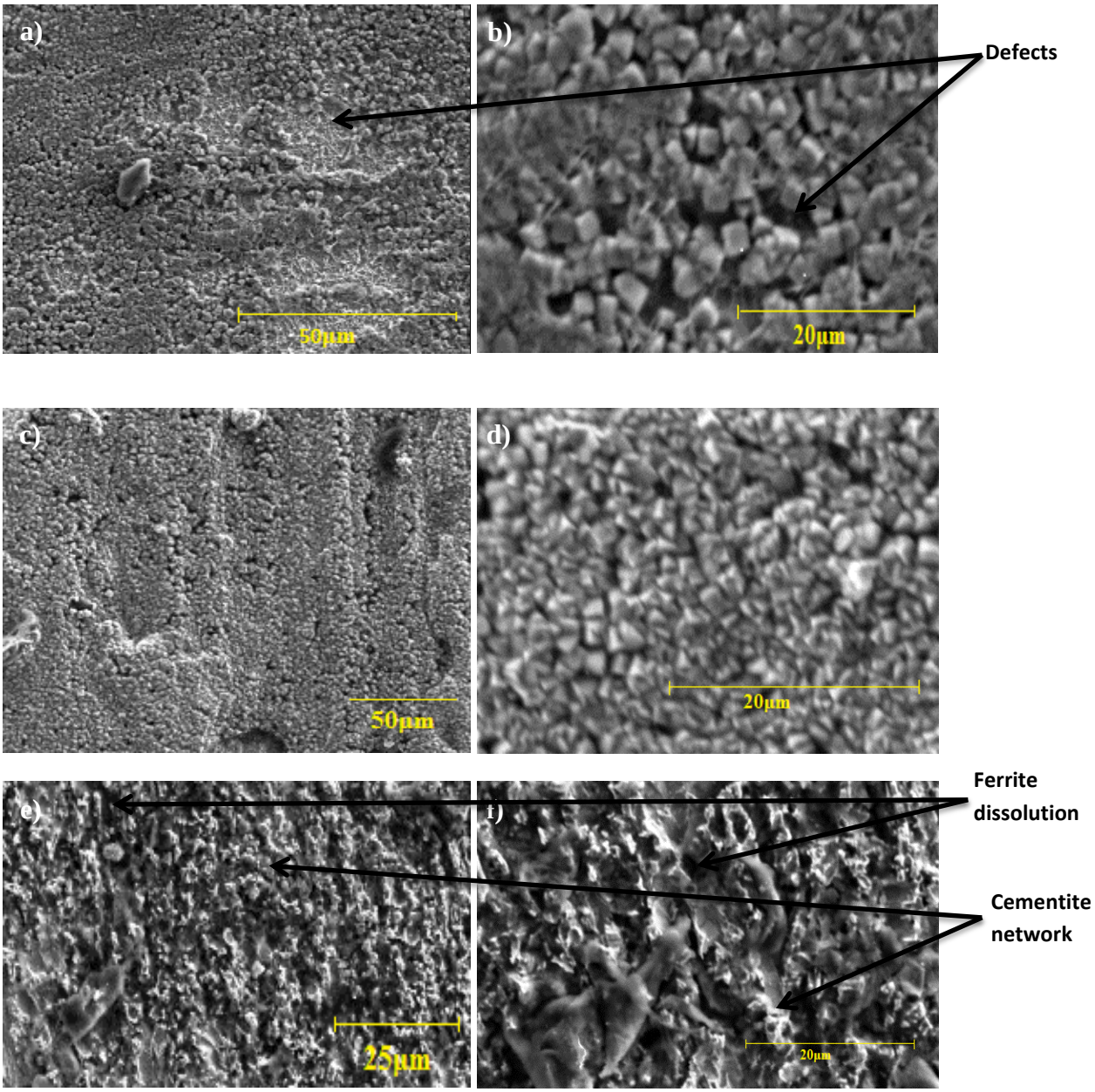

Fig. 4.4.1 SEM micrograph of a) PM, c) WM and e) HAZ at 250 X and b) PM, d) WM and e) HAZ AT 1000X after CO_2 corrosion

4.5 IMPLICATIONS OF RESULT OBTAINED

The HAZ had a high initial corrosion rate, which suggests that the rate of ferrite dissolution into the corrosive media was fast. A high initial Fe^{2+} concentration was responsible for the fast rate of $FeCO_3$ precipitation and surface deposition observed in the HAZ. This was seen by the drop in corrosion rate after 48 h of exposure. Corrosion rate in the WM was observed to decrease at a slow and steady pace until no corrosion was observed after 168 h. This suggests that the $FeCO_3$ precipitates formed in the WM took a longer time to form and formed a protective barrier against the corrosive media.

The cementite layer observed across the surface of the PM could indicate that Fe^{2+} dissolution occurred at a faster rate than $FeCO_3$ precipitation, leaving behind a web of Fe_3C which is non-protective as was evident in the high corrosion rate observed. This suggests that local acidification occurred at the Fe_3C sites, thereby promoting galvanic corrosion and increasing the rate of attack. Despite the exposure to high temperature and pH which favor a decrease in $FeCO_3$ solubility limit, the precipitation of $FeCO_3$ in the parent metal was not observed. This suggests that the microstructure plays an important role in film formation. The microstructure determines the carbide distribution which is essential in surface film stability or instability. The PM comprised a fine distribution of pearlite grains (0.88 μm) which might not have been sufficient enough to provide the framework necessary to anchor $FeCO_3$ precipitates. The HAZ had an average pearlite grain size of 2.23 μm while that of the WM was 1.02 μm. The larger pearlite grain size in the HAZ might have been responsible for the fast formation of $FeCO_3$ precipitates by providing a larger surface area for precipitate anchoring.

SEM images show that the film formed across the surface of the HAZ contained inclusions as opposed to that of the WM, which took a longer time to form. These inclusions could act as sites for localized corrosion and could have been responsible for the slow drop in corrosion rate observed in the HAZ. The WM was observed to have a more compact passive film, which could either signify that the film had a larger thickness, or that $FeCO_3$ deposition was more uniform across the surface of the metal. This also suggests that adequate time is required for uniform deposition of $FeCO_3$ precipitates across the surface of a metal. SEM observation of the PM was synonymous with the corrosion rates obtained. The corrosion rate in the PM was seen to decrease at a lower rate as opposed to the WM and HAZ.

Chemical analysis revealed that the WM contained 0.169 wt.% Mo and 0.063 wt.% C, while that of the PM contained <0.002 wt.% Mo and 0.074 wt. % C. The drop in the carbon content in the WM was as a result of the addition of Mo, which has the tendency to form carbides thereby reducing the amount of C available in the steel. The increase in Mo was as a result of the filler metal used during the welding process (BA-S2Mo), which had a high Mo content. As an alloying element, Mo improves the pitting resistance and has been reported to aid passivation on the surface of a metal. However, there have been contradicting reports on the role of Mo in passivation. The chemical analysis was therefore not conclusive in determining if the chemical composition of the PM and WM was responsible for the variations in film formation observed.

CHAPTER 5: CONCLUSION AND FUTURE WORK

5.1 INTRODUCTION

In this work, the surface film formation across the welded joint of an X65 steel exposed to CO_2 corrosion was analyzed. The aim of the work was to analyze if variations in the microstructure across a weld would give rise to differences in the characteristics of the surface film that formed after exposure to the corrosive media under the same conditions. The porous cementite layer formed on the surface of the PM, as opposed to the WM and HAZ where $FeCO_3$ precipitates were seen, implied that despite the fact that pearlite provides anchorage for $FeCO_3$ precipitates, the pearlite grain size could determine the effectiveness of this anchorage. There is therefore need for researchers to determine the effective pearlite grain size range for precipitate anchoring. Adequate time is required for $FeCO_3$ precipitates to cover the entire surface of the metal, thereby providing a more efficient covering.

The above work was carried out with some limitations, which will necessitate further research. It was assumed that the only ions present in the corrosive media were CO_3^{2-} and Fe^{2+} and did not account for the presence of competing ions and/or crude oil in the media. Further work should therefore be carried out on the effect of competing ions and crude oil on the cathodic and anodic reactions and the rate of precipitation in order to better mimic the reactions which occur in the field.

It should be stated that the microstructures of the PM, WM and HAZ used in this research is only applicable to a metal having the same chemical composition and welded under the

same conditions employed in this research. Variations in microstructure and chemical composition will exist across various welded joints as it is dependent on several factors. Further research should therefore be carried out on the effect of various welding techniques on the microstructures of a welded joint.

REFERENCES

[1] M. Blunt, F. J. Fayers, and F. M. Orr, "CARBON DIOXIDE IN ENHANCED OIL RECOVERY MARTIN BLUNT, F. JOHN FAYERS and FRANKLIN M. ORR, JR. Department of Petroleum Engineering, Stanford University, Stanford, California 94305-2220, USA," *Energy Convers. Manag.*, vol. 34, no. 9, pp. 1197–1204, 1993.

[2] V. Alvarado and E. Manrique, "Enhanced Oil Recovery: An Update Review," *Energies*, vol. 3, no. 9, pp. 1529–1575, Aug. 2010.

[3] "[3] World Oil Production.pdf." pp. 293–295, 2000.

[4] C. Energy, "CO 2 Enhanced Oil Recovery."

[5] B. Y. S. Kokal, A. Al-kaabi, E. Advanced, and S. Aramco, "Enhanced oil recovery : challenges & opportunities," pp. 64–69, 2010.

[6] I. S. Cole, P. Corrigan, S. Sim, and N. Birbilis, "Corrosion of pipelines used for CO 2 transport in CCS: Is it a real problem?," *Int. J. Greenh. Gas Control*, vol. 5, no. 4, pp. 749–756, Jul. 2011.

[7] Y. S. Choi and S. Nešić, "Determining the corrosive potential of CO2 transport pipeline in high pCO2-water environments," *Int. J. Greenh. Gas Control*, vol. 5, no. 4, pp. 788–797, Jul. 2011.

[8] J. L. Mora-mendoza and S. Turgoose, "Fe 3 C influence on the corrosion rate of mild steel in aqueous CO 2 systems under turbulent flow conditions," *Corros. Sci.*, vol. 44, pp. 1223–1246, 2002.

[9] L. S. Moiseeva, "Carbon Dioxide Corrosion of Oil and Gas Field Equipment," *Prot. Met.*, vol. 41, pp. 82–90, 2003.

[10] F. M. Song, "A comprehensive model for predicting CO2 corrosion rate in oil and gas production and transportation systems," *Electrochim. Acta*, vol. 55, pp. 689–700, 2010.

[11] S. L. Wu, "Characterization of the surface film formed from carbon dioxide corrosion on N80 steel," *Mater. Lett.*, vol. 58, pp. 1076–1081, 2004.

[12] G. T. B. B.R. Linter, "Reaction of pipeline steels in carbon dioxide solutions," *Corros. Sci.*, vol. 41, pp. 117–139, 1999.

[13] I. S. B. A. B. Forero, Milagros.M.G. Nunez, "Analysis of the Corrosion Scales Formed on API 5L X70 and X80 Steel Pipe in the Presence of CO2," *Mater. Res.*, vol. 17, pp. 461–471, 2014.

[14] Y. Sun and S. Nesic, “A Parametric Study and Modeling on Localized CO2 Corrosion In Horizontal Wet Gas Flow,” *Corrosion*, no. 04380, pp. 1–24, 2004.

[15] S. N. S. D.A Lopez, T. Perez, “The Influence of microstructure and chemical composition of carbon and low alloy steels in CO2 corrosion. A state-of-the-art appraisal,” *Mater. Des.*, vol. 24, pp. 561–575, 2003.

[16] G. A. Z. J.B. Sun, “The formation mechanism of corrosion scale and electrochemical characteristics of low alloy steel in carbon dioxide-saturated solution,” *Corros. Sci.*, vol. 57, pp. 131–138, 2012.

[17] C. W. Du, X. G. Li, P. Liang, Z. Y. Liu, G. F. Jia, and Y. F. Cheng, “Effects of Microstructure on Corrosion of X70 Pipe Steel in an Alkaline Soil,” *J. Mater. Eng. Perform.*, vol. 18, no. 2, pp. 216–220, Aug. 2008.

[18] P. W. C-M Lee, S Bond, “Preferential Weld Corrosion: Effects of Weldment Microstructure and Composition.”

[19] M. J. R. K. Alawadhi, “Preferential Weld Corrosion of X65 Pipeline Steel in Flowing Brines Containing Carbon Dioxide.”

[20] “Basic Understanding of Weld Corrosion,” *Corros. Weldments*, no. Ref 1, pp. 1–13, 2006.

[21] M. A. Adegbite, S. A. Impey, and M. J. Robinson, “The Influence of Hydrodynamics on the Preferential Weld Corrosion of X65 Linepipe Steel in Flowing Brine Containing Carbon Dioxide,” *Corrosion*, 2014.

[22] S. Bond, “Corrosion of Welded Components in Marine Environments,” *Prev. Manag. Mar. Corros.*, 2003.

[23] J. F. Wallace, “A review of welding cast steels and its effects on fatigue,” *Steel Founders’ Soc.*, pp. 1–90, 1979.

[24] N. Bailey, “Submerged Arc Welding Ferritic Steels with Alloyed Metal Powder,” *Am. Weld. Soc.*, vol. 41, no. August, 1991.

[25] S. N. Omkar A. Nafday, “Iron Carbonante Scale Formation and CO2 Corrosion in the Presence of Acetic Acid,” *Corrosion*, no. 05457, pp. 1–13, 2005.

[26] Y. J. Tan, S. Bailey, and B. Kinsella, “An Investigation of the Formation and Destruction of Corrosion Inhibitor Films Using Electrochemical Impedance Spectroscopy (EIS),” *Corros. Sci.*, vol. 38, pp. 1545–1561, 1996.

[27] Z. F. Yin, W. Z. Zhao, Y. R. Feng, and S. D. Zhu, “Characterisation of CO 2 corrosion scale in simulated solution with Cl – ion under turbulent flow conditions,” *Corros. Eng. Sci. Technol.*, vol. 44, no. 6, pp. 453–461, Dec. 2009.

[28] Z. F. Yin, X. Z. Wang, L. Liu, J. Q. Wu, and Y. Q. Zhang, "Characterization of Corrosion Product Layers from CO2 Corrosion of 13Cr Stainless Steel in Simulated Oilfield Solution," *J. Mater. Eng. Perform.*, vol. 20, no. 7, pp. 1330–1335, Oct. 2010.

[29] J. Zhang, Z. L. Wang, Z. M. Wang, and X. Han, "Chemical analysis of the initial corrosion layer on pipeline steels in simulated CO2-enhanced oil recovery brines," *Corros. Sci.*, vol. 65, pp. 397–404, Dec. 2012.

[30] J. K. Heuer and J. F. Stubbins, "An XPS characterization of FeCO 2 Films from CO2 corrosion," *Corros. Sci.*, vol. 41, pp. 120–132, 1998.

[31] A. Pfennig, B. Linke, and A. Kranzmann, "Corrosion behaviour of pipe steels exposed for 2 years to CO 2-saturated saline aquifer environment similar to the CCS-site Ketzin, Germany," *Energy Procedia*, vol. 4, pp. 5122–5129, 2011.

[32] Z. F. Yin, W. Z. Zhao, W. Y. Lai, C. X. Yin, and S. D. Zhu, "Film Characteristics of Carbon Steel in Simulant Solution with the Effect of Acetic Acid and CO2," *J. Mater. Eng. Perform.*, vol. 19, no. 5, pp. 693–699, Aug. 2009.

[33] S. D. Zhu, G. S. Zhou, J. Miao, R. Cai, and J. F. Wei, "Mechanical properties of CO 2 corrosion scale formed at different temperatures and their relationship to corrosion rate," *Corros. Eng. Sci. Technol.*, vol. 47, no. 3, pp. 171–177, May 2012.

[34] O. Kalogirou, G. Stergioudis, O. Haidar, and D. Tsipas, "Identification of corrosion products resulting from accelerated oxidation process," *Corros. Eng. Sci. Technol.*, vol. 44, no. 6, pp. 469–473, Dec. 2009.

[35] G. a. Zhang and Y. F. Cheng, "Micro-electrochemical characterization of corrosion of welded X70 pipeline steel in near-neutral pH solution," *Corros. Sci.*, vol. 51, no. 8, pp. 1714–1724, Aug. 2009.

[36] G.S. Das, "Precipitation and Kinetics of Ferrous Carbonate In Simulated Brine Solution and Its Impacts on CO2 Corrosion of Steel," *Int. J. Adv. Eng. Technol.*, 2014.

[37] K. Gao, F. Yu, X. Pang, G. Zhang, L. Qio, and W. Chu, "Mechanical properties of CO2 corrosion product scales and their relationship to corrosion rates," *Corros. Sci.*, vol. 50, pp. 2796–2803, 2008.

[38] N. Sato, "Basics of Corrosion Chemistry," in *Green Corrosion Chemistry and Engineering: Opportunities and Challenges*, Wiley-VCH, 2011, pp. 1–32.

[39] K.A. Natarajan, "Corrosion : Introduction – Definitions and Types," in *Advances in Corrosion Engineering*, pp. 1–9.

[40] J. R. Sully and D. W. Taylor, "Electrochemical Methods of Corrosion Testing," *Met. Handb.*, vol. 37, 1987.

[41] M. P. Groover, “Fundamentals of welding,” *Fundam. Mod. Manuf. Mater. Process. Syst.*, no. 1, pp. 1–10, 2010.

[42] “Metal Welding - Types and Processes,” pp. 1–4.

[43] J. Hernandez and J. Genesca, “Formation of iron-carbonate scale-layer and corrosion mechanism of API x7o pipeline steel in carbon dioxide-satuated 3% sodium chloride,” pp. 251–258, 2012.

[44] R. Rodrigues, E. Tonella, and K. Althoff, “Continuous Fermentation of Sugar Cane Syrup Using Immobilized Yeast Cells,” *J. Biosci. Bioeng.*, vol. 91, no. l, pp. 48–52, 2001.

[45] M. Laguna-aguilar, M. S. Alvarado-moreno, O. S. Sánchez-, R. Ramírez-jiménez, E. A. Zárate-nahón, R. María, I. Fernández-salas, and E. A. Rebollar-téllez, “Field Evaluation of a Novel Trap Baited with Carbon Dioxide Produced bu Yeast for the Collection of Female Aedes Aegypti Mosquitoes in Mexico,” *Southwest. Entomol.*, vol. 37, no. 4, 2012.

[46] R. C. Smallegange, W. H. Schmied, K. J. Van Roey, N. O. Verhulst, J. Spitzen, W. R. Mukabana, and W. Takken, “Sugar-fermenting yeast as an organic source of carbon dioxide to attract the malaria mosquito Anopheles gambiae,” *Malar. J.*, vol. 9, no. 1, p. 292, 2010.

[47] W. D. Callister and J. Wiley, *Materials Science*. pp. 622–651.

[48] A. Dugstad, “Fundamental Aspects of CO2 Metal Loss Corrosion Part l: Mechanism,” *Corrosion*, no. 06111, pp. 1–18, 2006.

[49] G. Schmitt and M. Hörstemeier, “FUNDAMENTAL ASPECTS OF CO2 METAL LOSS CORROSION - PART II: INFLUENCE OF DIFFERENT PARAMETERS ON CO2 CORROSION MECHANISMS,” *Corrosion*, pp. 1–26, 2006.

[50] M. B. Kermani and A. Morshed, “Carbon Dioxide Corrosion in Oil and Gas Production — A Compendium,” *Corrosion*, vol. 59, no. 8, pp. 659–683, 2003.

[51] M. H. Nazari, S. R. Allahkaram, and M. . Kermani, “The effects of temperature and pH on the characteristics of corrosion products in CO2 corrosion of grade X70 steel,” *Mater. Des.*, vol. 31, pp. 3559–3563, 2010.

[52] M. B. Kermani and D. Harrop, “The Impact of Corrosion on Oil and Gas Industry,” *SPE Production & Facilities*, vol. 11. 1996.

[53] R. F. Metcalfe, “Effects of Impurities on Minimum Miscibility Pressures and Minimum Enrichment Levels for CO2 and Rich Gas Displacements,” *Soc. Pet. Eng. J.*, pp. 219–224, 1982.

[54] J. Kvarekval, R. Nyborg, and M. Seiersten, “Corrosion product films on carbon steel in semi-sour CO2/H2S environments,” *Corrosion*, p. 02296, 2002.

[55] C. De Waard and D. E. Milliams, “CARBONIC ACID CORROSION OF STEEL.,” *Corrosion*, vol. 31. pp. 177–181, 1975.

[56] K. S. George and S. Nesic, “Investigation of carbon dioxide corrosion of mild steel in the presence of acetic acid - Part 1: Basic mechanisms,” *Corrosion*, vol. 63, pp. 178–186, 2007.

[57] C. De Waard and U. Lotz, “Prediction of CO2 corrosion of carbon steel,” in *CORROSION/93*, 1993, pp. 1–17.

[58] A. Dugstad, H. Hemmer, and M. Seiersten, “Effect of steel microstructure on corrosion rate and protective iron carbonate film formation,” *Corrosion*, vol. 57, pp. 369–378, 2001.

[59] T. Li, Y. Yang, K. Gao, and M. Lu, “Mechanism of protective film formation during CO2 corrosion of X65 pipeline steel,” *J. Univ. Sci. Technol. Beijing Miner. Metall. Mater. (Eng Ed)*, vol. 15, pp. 702–706, 2008.

[60] M. Nordsveen, S. Nešić, R. Nyborg, and A. Stangeland, “A mechanistic model for carbon dioxide corrosion of mild steel in the presence of protective iron carbonate films - Part 1: Theory and verification,” *Corrosion*, vol. 59, pp. 443–456, 2003.

[61] J. Kvarekval and A. Dugstad, “CORROSION MITIGATION WITH pH STABILISATION IN SLIGHTLY SOUR GAS/CONDENSATE PIPELINES,” *Corrosion*, no. 06646, pp. 1–15, 2006.

[62] T. Berntsen, M. Seiersten, and T. Hemmingsen, “Effect of FeCO3 Supersaturation and Carbide Exposure on the CO2 Corrosion Rate of Carbon Steel,” *Corrosion*, no. 11072, pp. 1–17, 2011.

[63] V. Hunnik, M. Pots, and A. Hendriksen, “THE FORMATION OF PROTECTIVE FeCO3 CORROSION PRODUCT LAYERS IN CO2 CORROSION,” *Corrosion*, 1996.

[64] D. Clover, B. Kinsella, B. Pejcic, and R. De Marco, “The influence of microstructure on the corrosion rate of various carbon steels,” *J. Appl. Electrochem.*, vol. 35, no. 2, pp. 139–149, Feb. 2005.